Batteries & Supercaps

Research Article
doi.org/10.1002/batt.202200526

Chemistry Europe
European Chemical Societies Publishing

www.batteries-supercaps.org

Efficient Low Temperature Performance of All Solid-State Zinc-Air Batteries with $MnCo_2O_4$/Carbon Fiber Bifunctional Electrocatalyst and Poly(Acrylic Acid) (PAA) Gel Polymer Electrolyte

Zahra Abedi,*[a] Jiayao Cui,[a] Weixing Chen,[a] and Douglas G. Ivey*[a]

Spinel type $MnCo_2O_4$ coated on asphaltene based carbon fibers ($MnCo_2O_4$/CF) was used as the electrode material/electrocatalyst for air electrodes for zinc-air batteries (ZABs). The batteries were assembled using an alkaline poly(acrylic acid) hydrogel electrolyte. The low temperature battery performance of the prepared ZAB cells was studied in terms of charge/discharge voltage and efficiency at different current densities, cycle life, power density, and cell voltage at temperatures between −45 °C and 21 °C. At all temperatures, the ZABs successfully completed 200 cycles of charge/discharge (100 h) at 2 mA cm^{-2} which is double the current density reported in the recent literature. The maximum power densities at 0 and −45 °C were 75 and 12 mW cm^{-2}, respectively. The good performance is attributed to the porous design of the air electrode and the use of an efficient electrocatalyst and an optimized gel polymer electrolyte.

Introduction

Development of new and sustainable energy storage devices has become crucial as the world is moving towards clean and sustainable energy. Rechargeable (secondary), zinc-air batteries (ZABs) have shown promising battery performance for use as alternative energy storage devices to traditional batteries like lithium-ion batteries.[1] Furthermore, ZABs are cost effective devices that benefit from safe operation and high energy density.[2] The main components of a ZAB cell are a metallic Zn electrode, an alkaline electrolyte, a separator, and an air electrode; the air electrode is often carbon based and contains electrocatalysts.[3,4] The name air electrode is taken from the air reactions that take place at this electrode. The oxygen reduction reaction (ORR) and oxygen evolution reaction (OER) occur at the air electrode during discharge and charge, respectively.[5] These reactions suffer from poor kinetics which results in problems like low battery voltage efficiency and poor cycling behavior.[6] This necessitates the use of effective electrocatalysts to improve the battery performance.[7]

Many effective electrocatalysts for use in ZABs have been developed. Transition metal oxides (TMOs), carbonaceous materials like graphite and carbon nanotubes, and precious metals like Pt, Ir and Ru are the most important materials that have shown promising catalytic behavior towards ORR and/or OER.[8–14] The cost, scarcity, and instability (in terms of battery cycling performance) of precious metals have made their widespread use in ZABs impractical.[15] Although TMOs have proven to be active towards ORR/OER, their insulating nature is an issue for energy storage devices. Carbon-based materials are used as conductive substrates for TMOs to improve charge transfer and conductivity issues.[5,10,14,16–18]

Carbon fibers have been shown to be excellent candidates for use in energy storage devices; they can be used as the conductive substrate for TMOs. Carbon fibers can be synthesized from various precursors like food scraps, polyaniline (PANI), and asphaltene. Asphaltene is viscous and high carbon content by-product of the oil sands industry with significantly more supply than demand. Melt-spinning can be employed to prepare micron-scale carbon fibers from asphaltene.[5,17,19–21]

In previous work by the authors, low-cost micron-scale carbon fibers were used as the air electrode material/electrocatalyst in ZABs with aqueous electrolytes. Spinel type $MnCo_2O_4$ coated on asphaltene derived carbon fibers ($MnCo_2O_4$/CF) was synthesized and homemade air electrodes were prepared using $MnCo_2O_4$/CF. The performance of the synthesized $MnCo_2O_4$/CF as the air electrode material in aqueous ZABs at room temperature was quite good in terms of battery efficiency and cycling stability.[5]

The design of the air electrode and the electrolyte are important parameters in addition to the electrocatalyst used, affecting the battery performance.[5,22] The air electrode has to be porous and the electrocatalyst needs to be well dispersed throughout the air electrode to allow for efficient oxygen penetration and adsorption during discharge. If the electrocatalyst used is not bifunctional (active towards both ORR and OER), two different electrocatalysts or two separate air electrodes could be used.[23] Aqueous and gel polymer electrolytes are often used in ZABs. Cell leakage, evaporation, and flooding are the main issues when using aqueous electrolytes.[24–26] Hydrogels are a category of gel polymer electrolytes that are capable of absorbing a significant amount of water without dissolving.

[a] Dr. Z. Abedi, J. Cui, Prof. W. Chen, Prof. D. G. Ivey
Department of Chemical and Materials Engineering
University of Alberta, Edmonton
Alberta, T6G 2V4 (Canada)
E-mail: sabedi@ualberta.ca
divey@ualberta.ca

Research Article
doi.org/10.1002/batt.202200526
Chemistry Europe
European Chemical Societies Publishing

Previous work has shown that when all the other components are the same, the use of a hydrogel electrolyte can lead to higher power densities and better battery performance. This was attributed to the higher viscosity of the hydrogel electrolyte compared with aqueous electrolytes, which resulted in less clogging of porosity and larger electrocatalyst/air/electrolyte contact area.[27] In addition, some recent studies have shown that the use of an effective gel polymer electrolyte can enhance the stability of the battery compared with aqueous electrolytes.[28,29]

The purpose of this work is to study the all solid state battery performance, at sub-zero temperatures, of ZABs made with $MnCo_2O_4$/CF as the air electrode material and alkaline poly(acrylic acid) hydrogel electrolyte.

Results and Discussion

Full cell battery charge/discharge tests at different current densities and temperatures for both Pt/RuO_2 and $MnCo_2O_4$/CF were conducted (Figure 1). It should be noted that the battery performance of $MnCo_2O_4$/CF at 21 °C and 0 °C completely overlap; i.e., there is no degradation in performance when the temperature is decreased to 0 °C. For cells prepared with either Pt/RuO_2 or $MnCo_2O_4$/CF, the performance of the battery degrades at all current densities as the temperature is decreased (except for $MnCo_2O_4$/CF at 0 °C). The charge voltage increases and the discharge voltage decreases, decreasing the battery efficiency. This is likely due to the reduced mobility of the charge carriers and increased viscosity of the hydrogel electrolyte.[30,31] Reduced mobility of the charge carriers, such as ions, leads to inefficient and reduced charge transfer and battery performance. The increase in the viscosity of the hydrogel electrolyte also negatively affects charge transfer efficiency and rate, which degrade the battery performance. As the electrolyte becomes more viscous, charge transfer becomes more difficult. Charge carrier mobility is further reduced as the electrolyte becomes more viscous. For example, the ZAB efficiency for Pt/RuO_2 and $MnCo_2O_4$/CF at 10 mA cm^{-2} at 0 °C are 56.2% and 55.8%, respectively, and at −25 °C are 44.4% and 34.4%, respectively. Reduced electrochemical reaction kinetics due to decreased mobility of charge transfer species and increased viscosity of the electrolyte at subzero temperatures are the main reasons for performance degradation. As the mobility of the charge carrier species decreases, collisions between the molecules decrease as well, leading to reduced reaction rates.[30]

Figure 1 also shows that the ZAB performance of $MnCo_2O_4$/CF at all temperatures and current densities is superior to that of Pt/RuO_2. As mentioned in the previous paragraph, the battery voltages for $MnCo_2O_4$/CF at 21 °C and 0 °C (curves in bright yellow and green in Figure 1b) completely overlap. $MnCo_2O_4$/CF is capable of charging/discharging without failure even at current densities as high as 20 mA cm^{-2} at all temperatures with the exception of −45 °C at 20 mA cm^{-2}. At −45 °C, $MnCo_2O_4$/CF can only perform at current densities $\leq$10 mA cm^{-2}. The lowest temperature at which Pt/RuO_2 can fully charge/discharge is −10 °C. At −45 °C, Pt/RuO_2 can only be operated at current densities $\leq$5 mA cm^{-2}. At −25 °C, the battery fabricated with Pt/RuO_2 can be discharged at all current densities, but the battery failed during the charging process at 20 mA cm^{-2}. It can be concluded that the superior catalytic behavior of $MnCo_2O_4$/CF to Pt/RuO_2 in aqueous electrolytes and at room temperature, that has been reported previously, is retained in gel polymer electrolytes and even at low temperatures.[5] Table 1 summarizes the charge and discharge voltages (E) shown in Figure 1 and Table 2 shows the efficiency and voltage gaps at current densities of 10 and 20 mA cm^{-2}.

Nyquist plots obtained from the solid state batteries made with $MnCo_2O_4$/CF and he PAA-KOH hydrogel electrolyte are presented in Figure 2. Figure 2(a) represents the EIS test results at all temperatures, while Figure 2(b and c) show expanded EIS plots at 21 °C and −45 °C, respectively. The solution resistance (R_s), which is determined from the first intercept of the plot with the x axis, increases as the temperature decreases. For example, R_s for $MnCo_2O_4$/CF at 21 °C is 1 Ω and at −45 °C is 12 Ω. The increase in solution resistance is due to the increase in viscosity of the gel polymer electrolyte as the temperature decreases. Diffusion of charge carrier species becomes less efficient as the viscosity of the electrolyte increases; this can

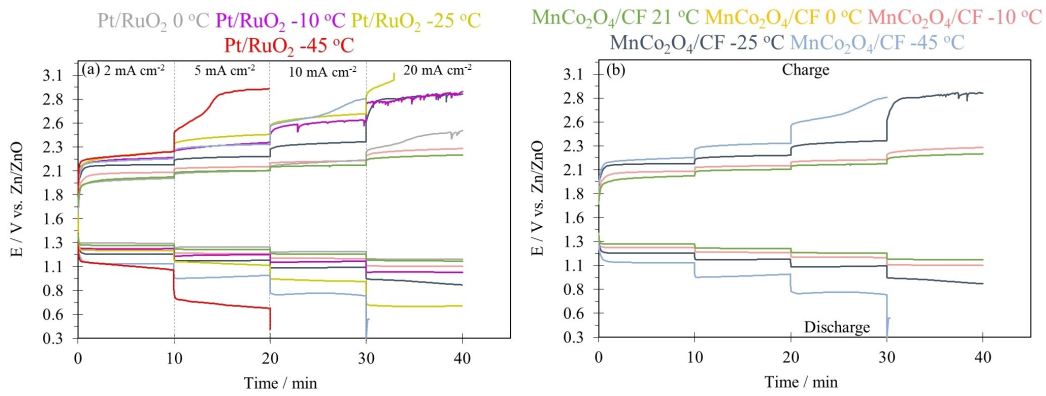

Figure 1. a) Full cell charge/discharge battery test results at a range of current densities and temperatures and b) expanded view of full-cell test results for $MnCo_2O_4$/CF.

Research Article
doi.org/10.1002/batt.202200526

Chemistry Europe
European Chemical Societies Publishing

Table 1. Battery full cell charge and discharge voltages for $MnCo_2O_4$/CF and Pt/RuO_2 at current densities of 10 and 20 mA cm^{-2}.

Sample	$MnCo_2O_4$/CF				Pt/RuO_2			
	$j = 10$ mA cm^{-2}		$j = 20$ mA cm^{-2}		$j = 10$ mA cm^{-2}		$j = 20$ mA cm^{-2}	
Temperature	Charge E [V]	Discharge E [V]	Charge E [V]	Discharge E [V]	Charge E [V]	Discharge E [V]	Charge E [V]	Discharge E [V]
Room temperature	1.98	1.25	2.03	1.21	2.04	1.25	2.15	1.18
0 °C	2.10	1.18	2.20	1.11	2.15	1.20	2.38	1.13
−10 °C	2.15	1.14	2.23	1.06	2.57	1.10	2.83	0.99
−25 °C	2.34	1.04	2.81	0.92	2.62	0.90	Exceeded cut-off	0.63
−45 °C	2.67	0.77	Exceeded cut-off	Exceeded cut-off	Exceeded cut-off	Exceeded cut-off	Exceeded cut-off	Exceeded cut-off

Table 2. Battery full cell efficiencies and voltage gaps for $MnCo_2O_4$/CF and Pt/RuO_2 at current densities of 10 and 20 mA cm^{-2}.

Sample	$MnCo_2O_4$/CF				Pt/RuO_2			
	$j = 10$ mA cm^{-2}		$j = 20$ mA cm^{-2}		$j = 10$ mA cm^{-2}		$j = 20$ mA cm^{-2}	
Temperature	Voltage gap [V]	Efficiency [%]	Voltage gap [V]	Efficiency [%]	Voltage gap [V]	Efficiency [%]	Voltage gap [V]	Efficiency [%]
Room temperature	0.73	63.1	0.82	59.6	0.79	61.3	0.97	54.9
0 °C	0.92	56.2	1.09	50.5	0.95	55.8	1.25	47.5
−10 °C	1.01	53.0	1.17	47.5	1.47	42.8	1.84	35.0
−25 °C	1.3	44.4	1.89	32.7	1.72	34.4	Failed	Failed
−45 °C	1.9	28.8	Failed	Failed	Failed	Failed	Failed	Failed

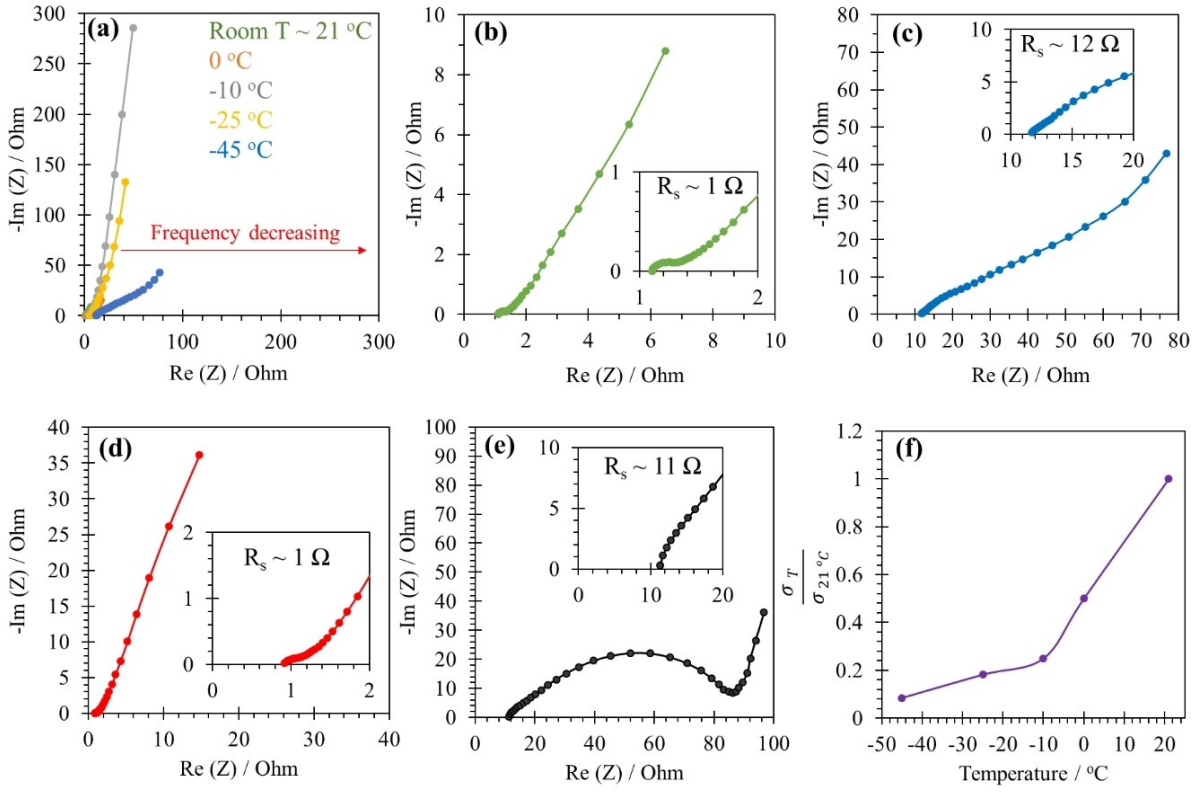

Figure 2. EIS test results for a) $MnCo_2O_4$/CF at different temperatures, b) $MnCo_2O_4$/CF at room temperature, c) $MnCo_2O_4$/CF at −45 °C, d) Pt/RuO_2 at room temperature and e) Pt/RuO_2 at −45 °C. f) Relative ionic conductivities for the hydrogel electrolytes at different temperatures.

negatively affect the battery performance and efficiency. The charge transfer resistance (R_{ct}) at the surface of the air electrode also increases due the higher viscosity and lower temperature. The battery tested at ~21 °C has a typical EIS plot with a semicircle in the high frequency region which enters the Warburg region (linear 45° line) as the frequency decreases. On the other hand, the battery tested at −45 °C does not enter the Warburg region until very low frequencies. Furthermore, the fact that the EIS plots move towards higher real portion values of the impedance (Re(Z)) as the temperature decreases indicates that diffusion is a limiting factor that degrades battery performance.

Research Article
doi.org/10.1002/batt.202200526
Chemistry Europe
European Chemical Societies Publishing

EIS tests for Pt/RuO_2 at 21 °C and −45 °C were conducted to confirm the hydrogel electrolyte resistance (R_s) and to evaluate diffusion in the Pt/RuO_2 battery system (Figure 2d and e). Electrolyte resistances at 21 °C and −45 °C were determined as ~1 Ω and ~11 Ω, respectively. These values are essentially the same as those determined from the $MnCo_2O_4$/CF EIS results. Comparing Figure 2b with 2d and 2c with 2e reveals that except for electrolyte resistance, the overall resistance values in the Pt/RuO_2 cell is higher than that in $MnCo_2O_4$/CF cell. The well-engineered design of the air electrode in the $MnCo_2O_4$/CF cell provides porosity and voids, which increase the three phase boundary area amongst air, electrolyte and electrocatalyst. This enhances the air reactions taking place at the air electrode, reducing the overall cell resistance.

The battery charge/discharge cycling behavior for $MnCo_2O_4$/CF and Pt/RuO_2 at room temperature and lower temperatures are presented in Figure 3 and Figure 4, respectively. Cycling tests at room temperature were conducted at a current density of 10 mA cm^{-2}, while 2 mA cm^{-2} was used for cycling tests at lower temperatures. For all temperatures, a cycling test included 10 min of discharge, 5 min of rest, and 10 min of charge followed by another 5 min of rest. Each cycling test had a duration of 100 h which is equal to 200 cycles.

At room temperature (Figure 3), $MnCo_2O_4$/CF in the PAA-KOH hydrogel electrolyte battery has stable charge/discharge cycling behavior, while Pt/RuO_2 in the PAA-KOH hydrogel electrolyte battery is unstable. The initial charge and discharge voltages for $MnCo_2O_4$/CF are 2.01 and 1.22 V vs. Zn/ZnO, respectively, which degrade to 2.16 and 1.12 V vs. Zn/ZnO, respectively, after 200 cycles. The initial and final battery efficiencies for this cell are 60.7% and 51.8%. The initial battery efficiency of the cell made with Pt/RuO_2 is 55.8% with 2.06 and 1.15 V vs. Zn/ZnO as the initial charge and discharge voltages, respectively. However, the discharge voltage of this battery reaches the cut-off voltage after ~70 cycles which causes cell failure. Due to poor battery performance of Pt/RuO_2 at room temperature, the cycling behavior of this cell was not investigated at lower temperatures.

For low temperature cycling (Figure 4), 2 mA cm^{-2} was chosen as the cycling current density in order to compare the results with the recent literature. Table 3 summarizes the voltage and efficiency values obtained from the cycling tests. Figure 4 and Table 3 indicate that battery performance degrades and battery efficiency is reduced as the temperature is decreased. For example, the initial battery efficiencies at 0, −10, −25 and −45 °C are 64.3%, 59.3%, 53.3%, and 45.2%, respectively. The performance degradation with decreasing temperature is a result of the reduced diffusion rate and reaction rate (due to reduced collisions between molecules) of the charge carrier species which lead to reduced electrochemical reaction kinetics and the increase in the viscosity of the electrolyte at subzero temperatures, as discussed previously. Even though lower temperatures negatively affect battery performance, the solid state battery made with $MnCo_2O_4$/CF in the PAA-KOH hydrogel electrolyte successfully completed 200 cycles even at −45 °C. The battery cycling performance is quite stable at temperatures as low as −25 °C, where the initial and final efficiencies are 53.3% and 49.1%, respectively. The periodic fluctuations in the charge and discharge voltages that are most pronounced at −45 °C are due to the temperature fluctuations (±3 °C) inside the freezer that were explained in the battery testing configuration section.

The power density and polarization curves for the battery prepared with $MnCo_2O_4$/CF in the PAA-KOH hydrogel electrolyte are presented in Figure 5. The maximum power output at

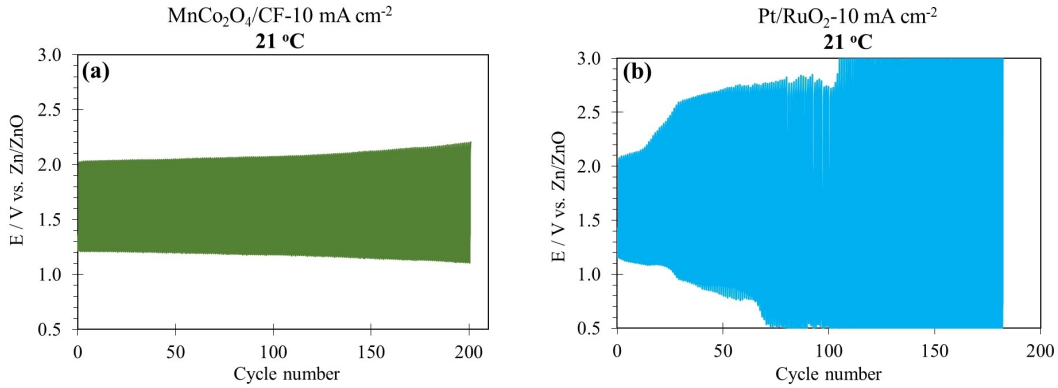

Figure 3. Cycling behavior of a) $MnCo_2O_4$/CF and b) Pt/RuO_2 in PAA-KOH hydrogel electrolyte at room temperature at 10 mA cm^{-2}.

Table 3. Initial and final battery voltages and efficiencies obtained from the cycling tests at low temperatures.

Temperature	Initial Charge *E* [V]	Discharge *E* [V]	Efficiency [%]	Final Charge *E* [V]	Discharge *E* [V]	Efficiency [%]
0 °C	1.96	1.26	64.3	2.09	1.21	57.9
−10 °C	2.04	1.21	59.3	2.11	1.18	55.9
−25 °C	2.12	1.13	53.3	2.22	1.09	49.1
−45 °C	2.21	1.00	45.2	2.50	0.84	33.6

Research Article
doi.org/10.1002/batt.202200526
Chemistry Europe
European Chemical Societies Publishing

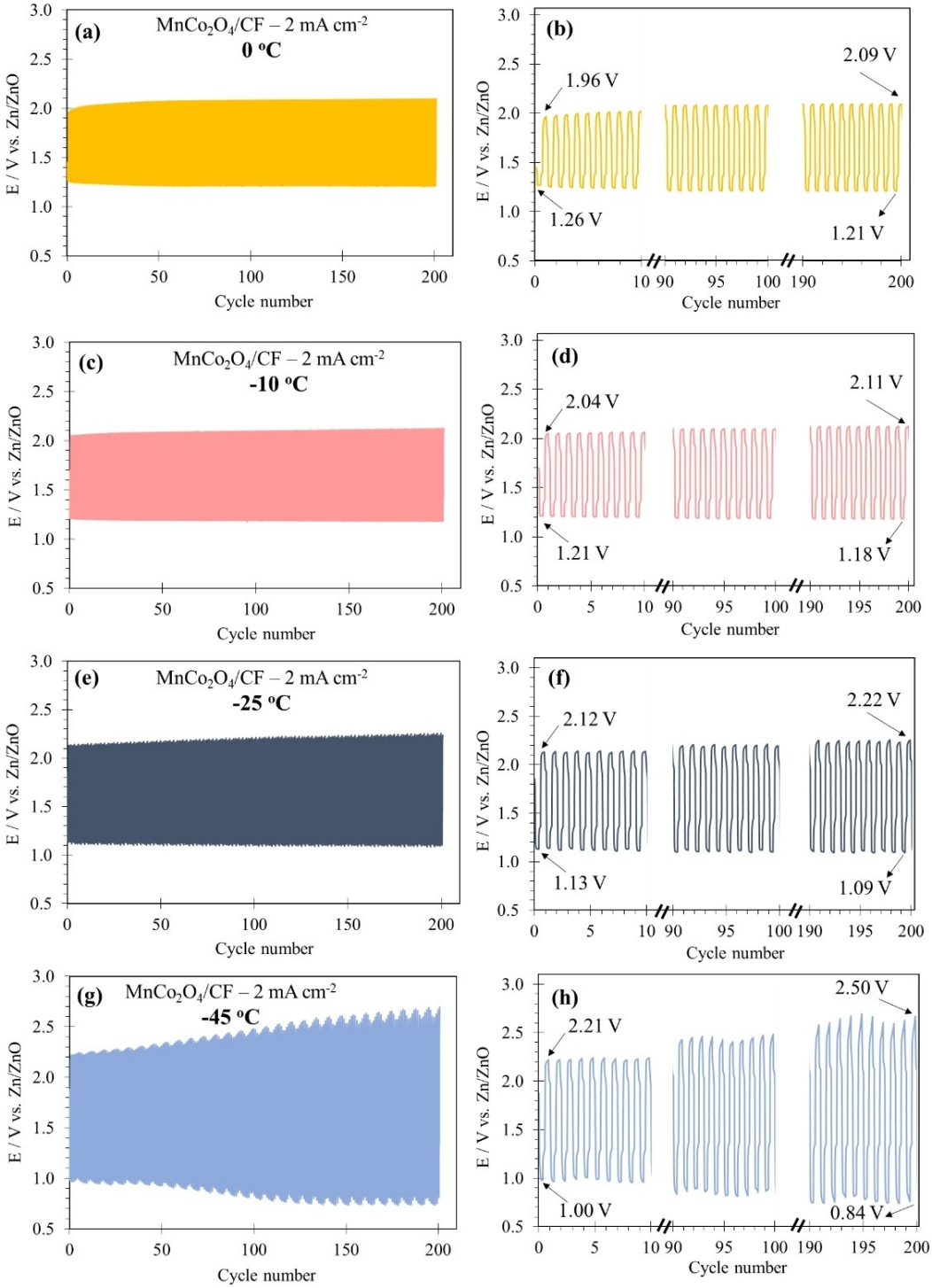

Figure 4. Cycling test results for $MnCo_2O_4$/CF in PAA-KOH hydrogel electrolyte at a and b) 0 °C, c and d) −10 °C, e and f) −25 °C, and g and h) −45 °C.

room temperature is ~240 mW cm^{-2} (Figure 5a). This value decreases to ~75 mW cm^{-2} at 0 °C.

At first glance, these results appear to contradict the rate test results shown in Figure 1(b), where the curves overlap for tests at both 21 °C and 0 °C. However, it should be noted that rate testing was only done at current densities up to 20 mA cm^{-2}. If the power densities for the 21 °C and 0 °C tests are compared for current densities less than 20 mA cm^{-2}, it is clear that the results overlap. The power density curves diverge at current densities exceeding 20 mA cm^{-2}. At higher current densities, the effect of viscosity becomes more apparent.

As the viscosity of the GPE increases, the reduced ion (OH^- and Zn^{2+}) or dissolved gas (O_2) diffusion rate negatively affects battery performance. Recent work showed that the effect of diffusion on battery performance is not significant at low current densities (e.g., $j < 5$ mA cm^{-2}), since the charge/dis-

Research Article
doi.org/10.1002/batt.202200526
Chemistry Europe
European Chemical Societies Publishing

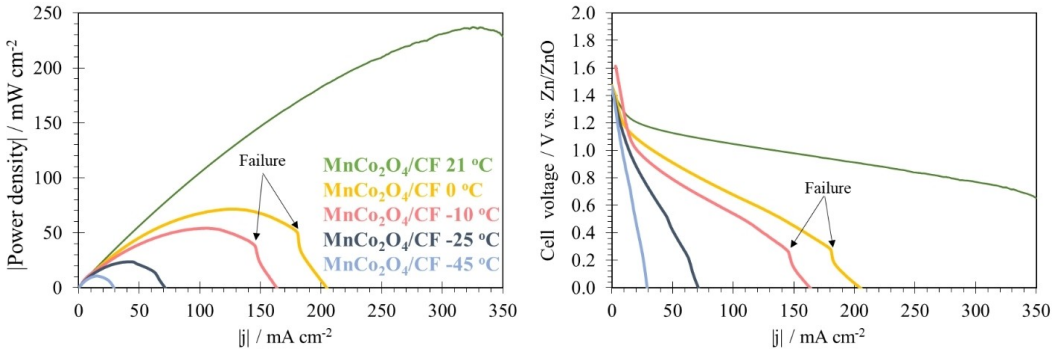

Figure 5. a) Power output and b) discharge polarization curves for $MnCo_2O_4$/CF in the PAA-KOH hydrogel electrolyte at different temperatures.

charge rates are slow enough to provide enough time for the diffusing species to move either towards or away from the air electrode. The effect of ion species diffusion becomes more significant at higher current densities (e.g., 50 mA cm^{-2}) as the diffusion rates are not fast enough to respond to the higher ORR/OER rates. As such battery performance degrades at 0 °C at current densities greater than ~20 mA cm^{-2}.[27,32] At 0 °C, the maximum current density applicable to the cell without causing failure is ~180 mA cm^{-2} while at room temperature the battery does fail even at 350 mA cm^{-2} (Figure 5a and b). Furthermore, the battery voltage drops more rapidly with increasing current density as the temperature decreases. For example, the minimum battery voltage at room temperature is ~0.67 V vs. Zn/ZnO (at 350 mA cm^{-2}), while at 0 °C this voltage drops to ~0.28 V vs. Zn/ZnO (at 180 mA cm^{-2}, just before failure) (Figure 5b). The degradation in power density and cell voltage as the temperature is decreased is attributed to the increase in viscosity of the electrolyte which also reduces the mobility of charge carriers as discussed previously. Table 4 summarizes the maximum power densities and current densities. Even though the power density, maximum current density and cell voltage decrease as the temperature is reduced, the battery performance is still superior to the work reported in the recent literature (Table 5).

Chen et al. employed a PAA-KOH based gel electrolyte and Pt/C and RuO_2 as the air electrode.[30] The current density used for the cycling tests was 1 mA cm^{-2} at 25 °C and −20 °C. The cells were tested for 100 cycles and the initial and final efficiencies of the cells were 79% and 52%, respectively, at 25 °C and 60% and 36%, respectively, at −20 °C. Furthermore, the maximum power density of the cells at 25 °C and −20 °C were reported as 10 and 8 mW cm^{-2}, respectively.[33] In the recent work reported by Zhang et al., all solid state ZAB cells were prepared with Pt/C-RuO_2 as the air electrode material and sodium polyacrylate-KOH as the electrolyte. The cells were tested at different temperatures of 25 °C and −20 °C. At 25 °C, the battery completed 86 cycles (29 h) at 1 mA cm^{-2} with initial and final efficiencies of 65% and 63%, respectively. The maximum power density at 25 °C was ~68 mW cm^{-2}. Reducing the temperature to −20 °C negatively affected the maximum power density (20 mW cm^{-2}) and efficiency; however, the battery was able to complete 133 cycles (44 h).[34] Jiang et al. assembled all solid state ZAB cells with Co_3O_4/RuO_2 and poly(2-acrylamido-2-methylpropanesulfonic acid)/polyacrylamide (PAMPS/PAAm) as the electrocatalyst and the electrolyte, respectively.[32] This battery was able to complete 177 cycles (60 h) at 25 °C at a current density of 1 mA cm^{-2}. The maximum power densities at 0 °C and 25 °C were 43 mW cm^{-2} and 57 mW cm^{-2}, respectively.[35] The work by An et al. introduced an effective all solid state ZAB cell with $NiCo_2O_4$ as the electrocatalyst and a PVA-KOH based gel electrolyte. The cell was successfully cycled for 33 h at 25 °C and 15 h at −10 °C at 1 mA cm^{-2}. The power output of the battery at 25 °C was 151 mW cm^{-2}; no power density at −10 °C was reported.[36] It is noteworthy that the zinc-air batteries in this work yielded superior results compared with those reported in the recent literature even though harsher testing conditions were used in this work. Current densities used in this work for full-cell and cycling tests are larger and the cycling durations are longer than most relevant recent works (Table 5) while providing stable battery performance with high power densities.

In summary, superior performing, all solid state ZABs (relative to the recent literature) were prepared with $MnCo_2O_4$/CF as the air electrode and a PAA-KOH based hydrogel electrolyte. The improved performance is attributed to the following reasons: 1) The use of micron-scale carbon fibers in

Table 4. Cell voltage, current density and power density values for $MnCo_2O_4$/CF in the PAA-KOH hydrogel electrolyte at different temperatures.

Temperature	Max j [mA cm^{-2}]	Max power density [mW cm^{-2}]
Room temperature	350	240
0 °C	180	75
−10 °C	150	50
−25 °C	70	25
−45 °C	30	12

Research Article
doi.org/10.1002/batt.202200526

Table 5. Comparison of low temperature zinc-air battery performance from this work with the recent literature.

Electrocatalyst	Temperature electrolyte	Current density [mA cm^{-2}]	Number of cycles-total cycling duration	Initial/final efficiency [%]	Maximum Power density [mW cm^{-2}]	Ref.
$MnCo_2O_4$/CF	21 °C PAA-KOH	10	200 cycles–100 h	63/56	240	This work
$MnCo_2O_4$/CF	0 °C PAA-KOH	2	200 cycles–100 h	64/58	75	This work
$MnCo_2O_4$/CF	−25 °C PAA-KOH	2	200 cycles–100 h	53/49	25	This work
Pt/C and RuO_2	−20 °C PAA-KOH	1	100 cycles-not provided	60/36	8	[33]
Pt/C and RuO_2	25 °C PAA-KOH	1	100 cycles-not provided	79/52	10	[33]
Pt/C and RuO_2	−20 °C Sodium polyacrylate-KOH	1	133 cycles–44 h	61/50	20	[34]
Pt/C and RuO_2	25 °C Sodium polyacrylate-KOH	1	86 cycles–29 h	65/63	68	[34]
Co_3O_4/RuO_2	0 °C PAMPS-KOH	1	5 cycles–1 h	51/50	43	[35]
Co_3O_4/RuO_2	25 °C PAMPS-KOH	1	177 cycles–~60 h	76/57	57	[35]
$NiCo_2O_4$	−10 °C PVA-KOH	1	15 h	55/50	Not provided	[36]
$NiCo_2O_4$	25 °C PVA-KOH	1	33 h	55/47	151	[36]

the fabrication of the air electrode provided porosity and voids. The design of the air electrode allowed for maximum three phase (air/electrolyte/electrocatalyst) boundary area to enhance the redox reactions at the air electrode at all temperatures. 2) The use of cost-effective carbon fibers as a conductive substrate for $MnCo_2O_4$ improved charge transfer at the air electrode. 3) The hydrogel electrolyte chemistry was optimized.[27]

Pristine and cycled air electrodes were characterized using a FE-SEM (Figure 6). Carbon fibers in the pristine material are completely coated with $MnCo_2O_4$ particles. The EDX maps for Mn and Co overlap completely which confirms mixed Mn–Co oxide formation (Figure 6a–d). This behavior was established in a previous study.[5] SEM/EDX analysis shows that after 200 cycles (100 h) of testing at both 0 °C and −45 °C, $MnCo_2O_4$ particles still coat the CFs in the electrodes (Figure 6e–l). Figure 6(m) shows EDX spectra for the pristine and cycled electrodes at −45 °C, taken from the entire image shown in Figure 6(a and i). The presence of K and Zn peaks for the cycled electrode is due to the zincate species and KOH in the electrolyte, precipitated as ZnO and KOH, on the surface of the electrodes. However, Mn and Co peaks are still visible after cycling at −45 °C for 100 h.

Conclusions

All solid state zinc-air battery (ZAB) cells were prepared using an efficient $MnCo_2O_4$/carbon fiber electrocatalyst and an alkaline poly(acrylic acid) (PAA) hydrogel electrolyte. The low temperature battery performance was evaluated in terms of charge/discharge voltages and efficiency, long term cycling stability, and power density. Battery tests were performed at room temperature, 0 °C, −10 °C, −25 °C, and −45 °C, with voltage efficiencies of ~63%, 53% and 30% (10 mA cm^{-2}) at room temperature, 0 °C and −45 °C, respectively. The performance was also superior to cells using Pt/RuO_2 as the air electrode catalyst. Long term cycling behavior was evaluated at 2 mA cm^{-2} at all test temperatures. The cells with $MnCo_2O_4$/carbon fiber air electrodes successfully completed 200 cycles (100 h) at all temperatures, while batteries prepared with Pt/RuO_2 failed after 70 cycles (35 h) at room temperature. The room and low temperature battery performance of batteries with $MnCo_2O_4$/carbon fiber electrocatalysts was superior to that reported in the recent literature in terms of the cycling life, efficiency, and power output (~240 and 75 mW cm^{-2} at room temperature and 0 °C, respectively), even though higher current densities and lower temperatures were used in this work compared with the most recent work. This study shows that the high performance of the prepared ZABs is due to the unique design of the air electrode, which utilize micron-scale $MnCo_2O_4$ coated carbon fibers that provide voids and macroporosity for efficient air electrode reactions.

Experimental Section

Bifunctional electrocatalyst synthesis

Asphaltene based carbon fibers were synthesized via the procedure reported in the recent literature.[21,37] The fibers were then coated with $MnCo_2O_4$ ($MnCo_2O_4$/CF) using a previously developed process and the coated fibers were used as the air electrode material in this work.[5] In summary, asphaltene derived fibers were carbonized at 1500 °C and then soaked in ~20 mL of 28 wt% NH_4OH for 10 min

Research Article
doi.org/10.1002/batt.202200526
Chemistry Europe
European Chemical Societies Publishing

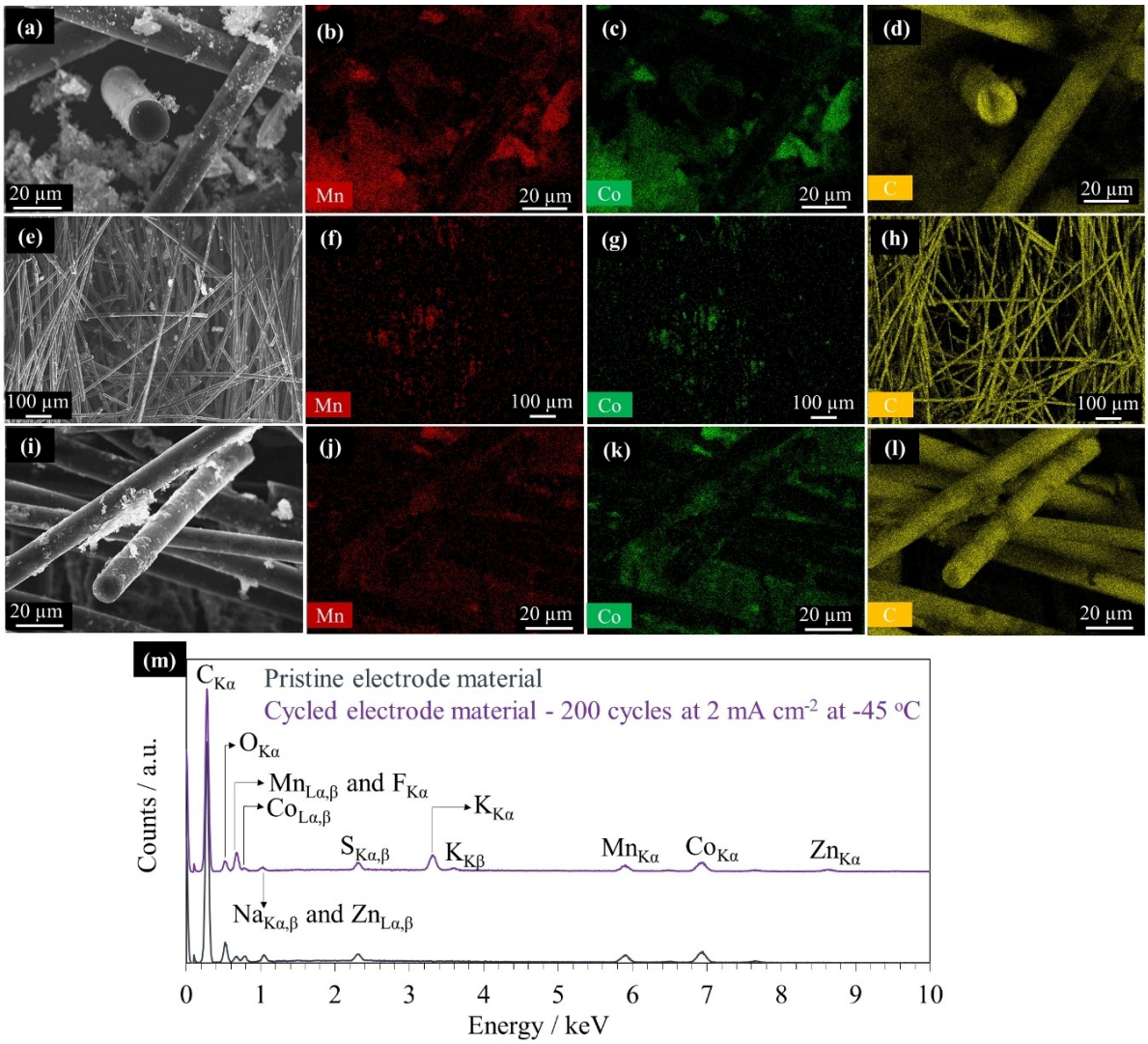

Figure 6. SEM/EDX analysis of $MnCo_2O_4$/CF electrodes. a–d) pristine, e–h) cycled at 0 °C, i–l) cycled at −45 °C, and m) EDX spectra from the electrodes.

followed by a 5 h sonication step to coat the fibers with $MnCo_2O_4$. The sonication solution contained 30 mL of reagent alcohol, 100 mg of NaOH, 166.67 mg of Mn(II) acetate ($Mn(Ac)_2$ or $C_4H_6MnO_4$), and 333.33 mg of Co(II) acetate ($Co(Ac)_2$ or $C_4H_6CoO_4$). $MnCo_2O_4$/CF was dried in a vacuum oven at 60 °C for 12 h after the sonication step.

The homemade air electrodes were prepared by pasting a mixture of 90 wt% $MnCo_2O_4$/CF, 5 wt% polytetrafluoroethylene (PTFE), and 5 wt% carbon black onto hydrophobic carbon paper (Fuel Cell Store: Toray Paper 060-TGP–H-060). The purpose of using the commercial carbon paper was to provide structural support for the electrocatalyst layer. The mass loading of $MnCo_2O_4$/CF on the carbon paper was ~10 mg cm^{-2}.

A mixture of 30 wt% Pt and 15 wt% RuO_2 combined with carbon black, purchased from Alfa Aesar, was used to prepare electrodes with the ORR/OER benchmark electrocatalyst (Pt/RuO_2) for electrochemical performance comparison with $MnCo_2O_4$/CF. A spray coating suspension, containing 50 mg of Pt-RuO_2 powder, 2 mL of deionized water, 0.1 mL of Nafion 5 wt%, and 1 mL of ethanol was prepared by sonicating the suspension for 30 min. The suspension was then spray coated on the same carbon paper with a mass loading of ~1 mg cm^{-2}.

A 30 min annealing step at 350 °C in a Lindberg/Blue M™ Moldatherm™ box furnace was employed for all prepared electrodes.

Electrolyte synthesis

Poly(acrylic acid) (PAA) was used as the host polymer for the solid state electrolyte. To prepare the alkaline hydrogel electrolytes, 6.5 M KOH, 0.5 M acrylic acid, 0.2 M ZnO, 30 mM N,N′-methylenebis(acrylamide) (MBAA), and 1.5 mM potassium persulfate ($K_2S_2O_8$ (KPS)) were mixed using a vortex mixer. MBAA and KPS were used as the crosslinker and the polymerization reaction thermoinitiator, respectively. The polymer precursor solution was kept at 60 °C in a vacuum oven for 1 h to allow the polymerization reaction to complete. The final hydrogel electrolyte was then cooled to room temperature overnight. KOH and ZnO were purchased from Fisher Scientific and acrylic acid, MBAA, and KPS were purchased from Sigma-Aldrich.

Battery testing configuration

Half-cell tests were conducted and the results published in a previous study dealing with the catalytic behavior of the electrocatalyst.[5] Zinc-air battery full cell testing was done by using the prepared air electrode as the working electrode and a 1 cm × 3 cm Zn sheet as the counter electrode. The synthesized PAA-KOH hydrogel was used as the electrolyte. A Ligfreezer Lo-Temp Equipment DW-60 W28 mini freezer was used for the low temperature battery tests. A thermometer was used to calibrate the temperature of the freezer; at any temperature, the temperature fluctuation was ±3 °C. Batteries were tested at room temperature (21 °C), 0 °C, −10 °C, −25 °C and −45 °C. The discharge/charge performance, battery efficiency, battery voltage, cycling behavior, and power values were investigated using the full cell set-up.

Electrochemical measurements

A Biologic VSP potentiostat was used to conduct the battery tests. Galvanostatic cycling with potential limitation (GCPL) tests were employed to measure the battery charge/discharge voltage at current densities of ±2, ±5, ±10, and ±20 mA cm^{-2}. The cut-off voltage for charge and discharge was 3.0 and 0.5 V vs. Zn/ZnO, respectively. Modular galvano (MG) tests with a current density (j) range of $-400 < j < 0$ mA cm^{-2} were used to measure the power output and the cell voltage and to study the maximum reachable current density without failure. The charge and discharge cut-off values were chosen as 3.0 and 0.5 V vs. Zn/ZnO, respectively. Battery failure was defined as either the charge voltage exceeding the upper cut-off voltage or the discharge voltage falling below the lower cut-off voltage. Electrochemical impedance spectroscopy (EIS) was utilized to measure the electrolyte resistance to investigate the battery performance in terms of diffusion of the charge carrier species. EIS tests for all samples were performed over a frequency range from 500 kHz to 50 mHz with an alternating potential amplitude of 5 mV.

Calculations

Voltage efficiencies were calculated from the full-cell tests as:

$$\text{efficiency} = V_{\text{discharge}}/V_{\text{charge}} \quad (1)$$

The ionic conductivities (σ) of the hydrogel electrolytes, at different temperatures, were calculated from the EIS tests as shown in Equation (2):

$$\sigma = \frac{l}{R_s A} \quad (2)$$

where l is the thickness (mm) of the hydrogel, R_s is the solution (hydrogel) resistance (Ω) and A is the area of hydrogel (cm^2). Since the thickness and area of the gel are constant at all temperatures due to the pressure exerted on the cell components, in the cell, ionic conductivities at all temperatures were normalized to the conductivity calculated at 21 °C.

Materials characterization

Field emission scanning electron microscopy (FE-SEM) coupled with energy dispersive X-ray (EDX) spectroscopy was used to study the microstructures and compositions of the pristine and cycled electrodes (ZEISS Sigma 300 VP-FE-SEM).

Acknowledgements

This work was financially supported by Alberta Innovates (Canada) through the Bitumen Beyond Combustion program and the Natural Sciences and Engineering Research Council (NSERC RGPIN-2018-04488) of Canada.

Conflict of Interest

The authors declare no conflict of interest.

Data Availability Statement

The data that support the findings of this study are available from the corresponding author upon reasonable request.

Keywords: bifunctional electrocatalyst · carbon fibers · gel polymer electrolyte · low temperature · $MnCo_2O_4$ · PAA · poly(acrylic acid) · solid-state · zinc-air batteries

[1] M. P. Clark, M. Xiong, K. Cadien, D. G. Ivey, *ACS Appl. Energ. Mater.* **2020**, *3*, 603–613.
[2] Z. C. Yao, T. Tang, J. S. Hu, L. J. Wan, *Energy Fuels* **2021**, *35*, 6380–6401.
[3] T. H. Park, J. S. Yeon, P. Sivakumar, Y. Kim, H. S. Park, *Int. J. Energy Res.* **2021**, *45*, 6698–6707.
[4] S. Clark, A. R. Mainar, E. Iruin, L. C. Colmenares, J. A. Bl'azquez, J. R. Tolchard, A. Latz, B. Horstmann, *J. Mater. Chem. A* **2019**, *7*, 11387–11399.
[5] Z. Abedi, D. Leistenschneider, W. Chen, D. G. Ivey, *Batteries & Supercaps* **2022**, *5*.
[6] M. Labbe, M. P. Clark, Z. Abedi, A. He, K. Cadien, D. G. Ivey, *Surf. Coat. Technol.* **2021**, *421*, 127390.
[7] J. Pan, X. L. Tian, S. Zaman, Z. Dong, H. Liu, H. S. Park, B. Y. Xia, *Batteries & Supercaps* **2019**, *2*, 336–347.
[8] A. McDougall, Z. Abedi, D. G. Ivey, *J. Appl. Electrochem.* **2021**, *1*.
[9] M. P. Clark, T. Muneshwar, M. Xiong, K. Cadien, D. G. Ivey, *ACS Appl. Nano Mater.* **2019**, *2*, 267–277.
[10] L. Li, J. Yang, H. Yang, L. Zhang, J. Shao, W. Huang, B. Liu, X. Dong, *ACS Appl. Energ. Mater.* **2018**, *1*, 963–969.
[11] J. M. Costa, M. P. Clark, A. F. de Almeida Neto, D. G. Ivey, *Int. J. Hydrogen Energy* **2020**, *45*, 16122–16132.
[12] Y. Li, H. Dai, *Chem. Soc. Rev.* **2014**, *43*, 5257–5275.
[13] S. Chen, S. Chen, J. Zhang, *Batteries & Supercaps* **2019**, *2*, 373–379.
[14] Y. He, Z. Abedi, C. Ni, S. Milliken, K. M. O'Connor, D. G. Ivey, J. G. C. Veinot, 2022.
[15] A. Muthurasu, S. H. Chae, T. Hoon Ko, P. Chandra Lohani, H. Yong Kim, *J. Colloid Interface Sci.* **2022**, *616*, 679–690.
[16] C. Guan, A. Sumboja, H. Wu, W. Ren, X. Liu, H. Zhang, Z. Liu, C. Cheng, S. J. Pennycook, J. Wang, *Adv. Mater.* **2017**, *29*.
[17] Z. Abedi, D. Leistenschneider, W. Chen, D. G. Ivey, *J. Electrochem. Soc.* **2022**, *169*, 010507.
[18] Q. Wang, Y. Xue, S. Sun, S. Yan, H. Miao, Z. Liu, *J. Power Sources* **2019**, *435*, 226761.
[19] Z. Abedi, D. Leistenschneider, W. Chen, D. G. Ivey, *Energy Technol.* **2020**, *2000588*, 1–11.
[20] D. Leistenschneider, Z. Abedi, W. Chen, D. G. Ivey, *Energy Fuels* **2022**.
[21] P. Zuo, D. Leistenschneider, Y. Kim, Z. Abedi, D. G. Ivey, Z. Zhang, W. Chen, *J. Ind. Eng. Chem.* **2021**, *104*, 427–436.
[22] P. Pei, K. Wang, Z. Ma, *Appl. Energy* **2014**, *128*, 315–324.
[23] P. Gu, M. Zheng, Q. Zhao, X. Xiao, H. Xue, H. Pang, *J. Mater. Chem. A* **2017**, *5*, 7651–7666.
[24] T. N. T. Tran, D. Aasen, D. Zhalmuratova, M. Labbe, H. J. Chung, D. G. Ivey, *Batteries & Supercaps* **2020**, *3*, 917–927.

[25] J. Park, M. Park, G. Nam, J. S. Lee, J. Cho, *Adv. Mater.* **2015**, *27*, 1396–1401.
[26] Z. Chen, W. Li, X. Yang, C. Ke, H. Chen, Q. Li, J. Guo, Y. He, Z. Guo, X. Liang, *J. Power Sources* **2022**, *523*, 231020.
[27] Z. Abedi, J. Cui, W. Chen, D. G. Ivey, *ACS Appl. Energ. Mater.* **2022**, *5*, 14164–14174.
[28] Y. Shao, J. Zhao, W. Hu, Z. Xia, J. Luo, Y. Zhou, L. Zhang, X. Yang, N. Ma, D. Yang, Q. Shi, J. Sun, L. Zhang, J. Hui, Y. Shao, *Small* **2022**, *18*.
[29] Y. Tian, S. Chen, S. Ding, Q. Chen, J. Zhang, *Chem. Sci.* **2022**, *14*, 331–337.
[30] Z. Karpas, Z. Berant, O. Shahal, *J. Am. Chem. Soc.* **1989**, *111*, 6015–6018.
[31] A. Guttman, J. Horváth, N. Cooke, *Anal. Chem.* **1993**, *65*, 199–203.
[32] M. R. Gennero De Chialvo, A. C. Chialvo, *J. Electroanal. Chem.* **1996**, *415*, 97–106.
[33] R. Chen, X. Xu, S. Peng, J. Chen, D. Yu, C. Xiao, Y. Li, Y. Chen, X. Hu, M. Liu, H. Yang, I. Wyman, X. Wu, *ACS Sustainable Chem. Eng.* **2020**, *8*, 11501–11511.
[34] Y. Zhang, Y. Chen, M. Alfred, F. Huang, S. Liao, D. Chen, D. Li, Q. Wei, *Composites Part B* **2021**, *224*, 109228.
[35] D. Jiang, H. Wang, S. Wu, X. Sun, J. Li, *Small Methods* **2022**, *6*, 1–9.
[36] L. An, B. Huang, Y. Zhang, R. Wang, N. Zhang, T. Dai, P. Xi, C. H. Yan, *Angew. Chem.* **2019**, *131*, 9559–9563; *Angew. Chem. Int. Ed.* **2019**, *58*, 9459–9463.
[37] D. Leistenschneider, P. Zuo, Y. Kim, Z. Abedi, D. G. Ivey, A. D. Klerk, X. Zhang, W. Chen, *Carbon Trends* **2021**, *5*.

Manuscript received: December 5, 2022
Revised manuscript received: January 31, 2023
Accepted manuscript online: February 2, 2023
Version of record online: February 14, 2023